

**Electronic properties of hybrid organic–inorganic semiconductors**

B. Fluegel, Y. Zhang, and A. Mascarenhas

*National Renewable Energy Laboratory, Golden, Colorado 80401, USA*

X. Huang and J. Li

*Department of Chemistry and Chemical Biology, Rutgers University, Piscataway, New Jersey 08854, USA*

(Received 10 June 2004; published 8 November 2004)

Hybrid semiconductors comprising networks of inorganic II–VI semiconductor segments bonded to organic solvent chains show promise as a versatile material system that offers the capability of synthesizing many new electronic structures that are desirable for photonic applications. Polarized optical absorption and reflection are measured in single crystal semiconductor nanostructures composed of arrays of monolayers or linear chains. This shows very sharp spectral signatures of excitonic transitions, providing evidence of an electronic band-structure that is strongly modified from the bulk inorganic semiconductor. Together with x-ray diffraction structural analysis, it gives a clear image of a monolayer multiple quantum well structure in which a chemical growth process has achieved a quantum confinement larger than other known heterostructure types, together with near-zero layer width fluctuations, a very large oscillator strength and large exciton binding energy.

DOI: 10.1103/PhysRevB.70.205308

PACS number(s): 81.07.Pr, 81.05.Dz, 73.21.Fg, 73.21.Hb

**I. INTRODUCTION**

In the past three decades, a key technological achievement in materials physics has been tailoring the electronic confinement in epitaxially grown semiconductor heterostructures for specific device applications such as lasers, light emitting diodes, and solar cells. Because it is crucial to match the lattice constants of the epilayer material and its sublayer, the design of such heterostructures is guided, and limited, by the available semiconductor band gaps and lattice constants. The gradual exhaustion of usable new inorganic material combinations has motivated searches for *organic–inorganic* semiconductor epitaxial heterostructures. As recently pointed out,<sup>1</sup> the lattice-matching constraint can be greatly relaxed for an organic epilayer, and dramatically new properties can be obtained. Concomitantly, chemical techniques have made great progress in replacing complex deposition machinery. Based on a suitable chemical reaction (e.g., solvothermal or solution growth), inorganic semiconductor crystal segments can self-assemble into regular networks linked by insulating organic molecules on an atomic scale. The method is very tailorable, and by varying cation, anion, as well as the length of the organic spacer, many new materials have been synthesized, in layered perovskites,<sup>2–4</sup> and in some of the well-known II–VIs.<sup>5–11</sup> The latter has been demonstrated<sup>6</sup> to be a very flexible system that can form large extended networks of both planar and line (wire) segments. Direct optical evidence of their electronic structure, e.g., absorption, has been rare since most growth methods suffer from limitations of thickness, lateral size, or domain size. Our synthesis of over 30 new II–VI heterostructures includes some that readily form stable, macroscopic, single crystal specimens. Using optical studies we show that these hybrid materials exhibit remarkably strong confinement-induced behavior: very strong absorption in a sharp exciton-like line series, accompanied by a giant confinement energy and exciton binding energy, and a large refractive index and anisotropy near the band edge. These results demonstrate a

method of tailoring electronic band gaps which is independent of semiconductor alloying or deposition accuracy and free from the inevitable alloy fluctuations. It significantly enhances the combinations of energy band gaps and lattice constants available for electronic applications.

Organic chains terminating in amine (NH<sub>3</sub>) groups have proven particularly adept at networking a II–VI zincblende or wurtzite crystal into periodic arrays of wires or monolayers. The samples used for this study include  $\beta$ -ZnTe(en)<sub>1/2</sub>, (en=ethylenediamine),<sup>5</sup> composed of monolayers of ZnTe extended into a periodic three-dimensional lattice by spacers of ethylenediamine, as shown in Fig. 1. Its monolayer is a distorted (110) plane of zincblende ZnTe and the spacers are single en molecules covalently bonded to the two Zn atoms in neighboring planes, creating a homogeneous and structurally rigid crystal. This contrasts with the layered perovskites where each inorganic layer is hydrogen-bonded to its own two layers of spacer molecules, above and below the inorganic. This three-layer basis is then repeated via a weak van der Waals attraction between two adjacent spacers that can easily be broken. Our II–VI material system actually includes examples of both schemes since different growth conditions can result in either fully bonded or “coordinating” layers. Because of this important distinction, we refer to them respectively as 3D and 2D, independent of their quasi-two-dimensional electronic character. Additionally, we have studied a 1D sample, ZnTe(pda)<sub>1/2</sub>, in which a change of growth conditions and solvent, propanediamine (pda), results in an array of coordinated ZnTe wires<sup>6</sup> as shown in Fig. 2. Our measurements of the low-temperature reflection and transmission of single-crystal platelets at the fundamental absorption edge reveals the optical properties of these two samples with respect to their confined geometry.

**II. EXPERIMENT**

Single crystals of  $\beta$ -ZnTe(en)<sub>1/2</sub> and ZnTe(pda)<sub>1/2</sub> were reaction grown and their structures determined as discussed

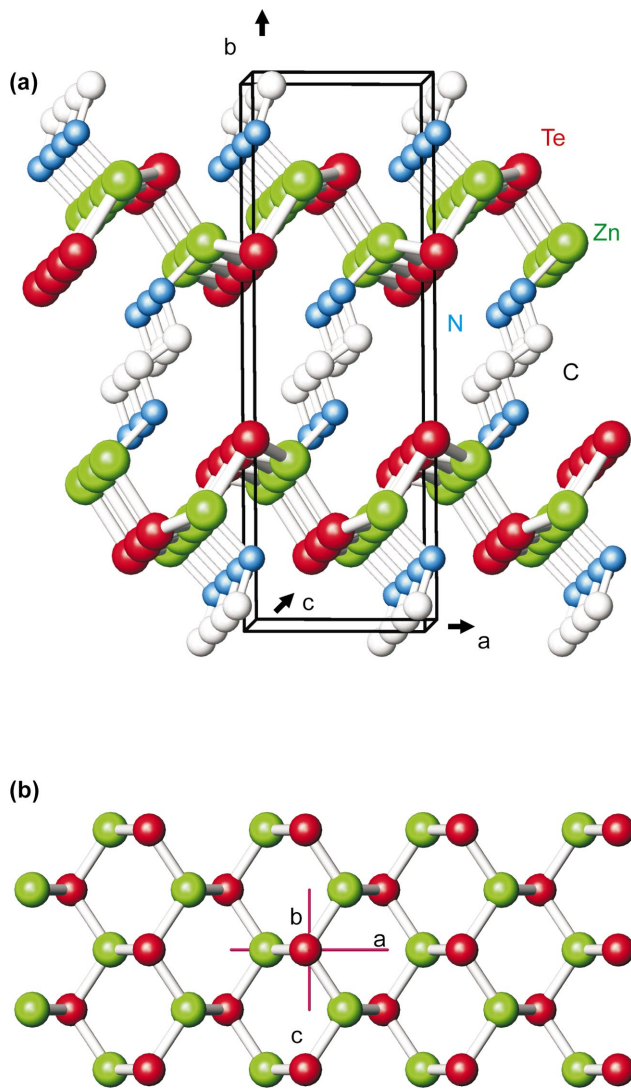


FIG. 1. (Color) 3D sample structure determined by x-ray diffraction (see data from Ref. 5). (a) Multiple ZnTe layers bonded by ethylenediamine chains attached at Zn atoms. Hydrogen atoms are omitted for clarity and the unit cell is shown, (b) a single ZnTe layer projected along *b* axis. Samples grow in thin platelets parallel to this figure, with edges oriented along the *a*- and *c*-axes.

in Refs. 5 and 6. The thinnest crystals from this process (typically  $80 \times 80 \times 1 \mu\text{m}$ ) were attached by a single corner to a He vapor cryostat and illuminated with the collimated and polarized output of a deuterium lamp. For measuring transmission in spectral regions of strong absorption, the  $\text{D}_2$  lamp was replaced with a frequency doubled, 100-fs-optical parametric oscillator that has a bandwidth of a few nm. No optical damage occurred at a fluence of  $10^{-10} \text{ J/cm}^2$ . Transmitted or reflected signal was detected with a spectrometer and cooled CCD detector array.

Samples to be etched were attached to glass coverslips using black wax, then immersed in 30%  $\text{H}_2\text{O}_2$ . Etching was conducted in a polarizing microscope to provide a relative measure of the remaining sample thickness. Final thickness was estimated by comparing multiple reflection spectral peaks to larger samples where the edge thickness could be measured by optical or electron microscope.

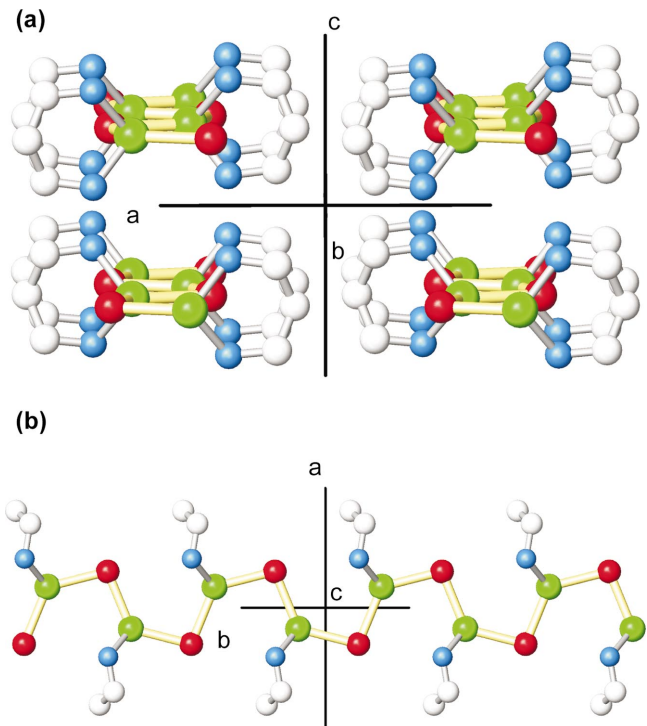


FIG. 2. (Color) 1D sample structure from x-ray diffraction, discussed in Ref. 6. (a) Four linear chains of ZnTe are shown coordinated by molecules of propanediamine; (b) top view of a single chain.

Refractive indices were obtained from the transmission peaks due to multiple reflections at the sample surfaces. The integer values of  $m$ , determining the transmission maxima at  $m\lambda = 2dn(\lambda)$ , where  $d$  is the thickness,  $n$  is the index, and  $\lambda$  the wavelength, were calibrated by separate measurements of the Brewster's angle at 633 and 458 nm. This simple ellipsometry approximately measures the in-plane refractive indices and ignores the weak dependence on the birefringence orthogonal to the platelet. The approximation was justified by a similar measurement on the sample edge which found the orthogonal index to be  $2.3 \pm 0.25$  at 633 nm, i.e., comparable to the in-plane indices.

### III. RESULTS

The  $\beta\text{-ZnTe(en)}_{1/2}$  3D platelets grow oriented normal to the monolayer stacking direction, **b** of Fig. 1. The low-temperature reflectivity for light propagating in this direction is shown in Fig. 3(a). A series of four derivative-shaped features is seen with zero crossings at 3.721, 3.752, 3.870, and 3.890 eV, labeled A–D. Their linewidths are quite sharp, comparable to high-quality inorganic semiconductors. In general, fitting such line shapes is complex. Critical point energies may correspond to different parts of the derivative-shaped feature, depending on the influence of various surface effects. However, even with this uncertainty, the spectrally sharp features allow identification sufficiently precise for our discussion.

Noting the transparency below 3.7 eV (shown below), we identify peaks A and B as free excitons associated with a

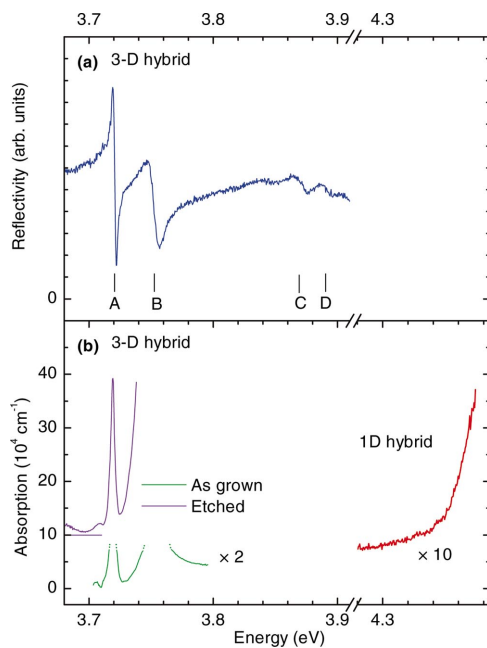


FIG. 3. (Color) 1.6 K optical reflectivity and absorption spectra. (a)  $E_{\parallel a}$  reflectivity of a freestanding, as-grown 3D sample with a thickness of  $0.9 \mu\text{m}$ . Four resonances are identified at A–D; (b) absorption for the same as-grown sample and a second 3D sample that has been etched to a thickness of  $\sim 0.2 \mu\text{m}$ . Etched samples were mounted on glass and typically blueshifted 10–20 meV by strain; data have been shifted by comparison with the freestanding sample. Right of axis break: unpolarized absorption of a freestanding 1D (wire) sample with a thickness of several microns. High absorption regions are limited by the experimental dynamic range; close examination of the 3D sample with a scanning double spectrometer found the peak absorption is still unresolved at greater than  $1.8 \times 10^5 \text{ cm}^{-1}$

split valence band at the fundamental direct energy gap. This is confirmed by continuous wave photoluminescence, in which the highest energy exciton peak occurs at 3.719 eV (not shown), and it is also confirmed by the optical absorption in Fig. 3(b). Two absorption peaks that exceed our dynamic range are seen at energies matching A and B. Investigation of many such samples confirms that this is a bulk phenomenon, that the absorption is very high, and its measurement in micron-thick samples is limited by stray light rejection, as discussed in Ref. 12. By using a much thinner etched sample we have been able to resolve the A peak with a narrow linewidth of  $< 4 \text{ meV}$  as shown in Fig. 3(b). The B peak, although observable, is still unresolved (not shown). At higher spectral energies, the very strong absorption continues to increase beyond the levels shown, preventing direct identification of the continuum band edge absorption. Compared to bulk ZnTe, where the free exciton energy is 2.4 eV, the transitions in Fig. 3 represent an enormous 1.3 eV shift of the absorption edge from the green into the ultraviolet spectral region. As we will discuss below, this shift is significantly beyond what can be achieved in inorganic quantum wells, and larger even than in typical semiconductor quantum dots or other hybrid organic–inorganic structures.

Both the absorption and reflectivity are highly anisotropic, even within the plane of the monolayers: for  $E_{\parallel c}$ , the absorp-

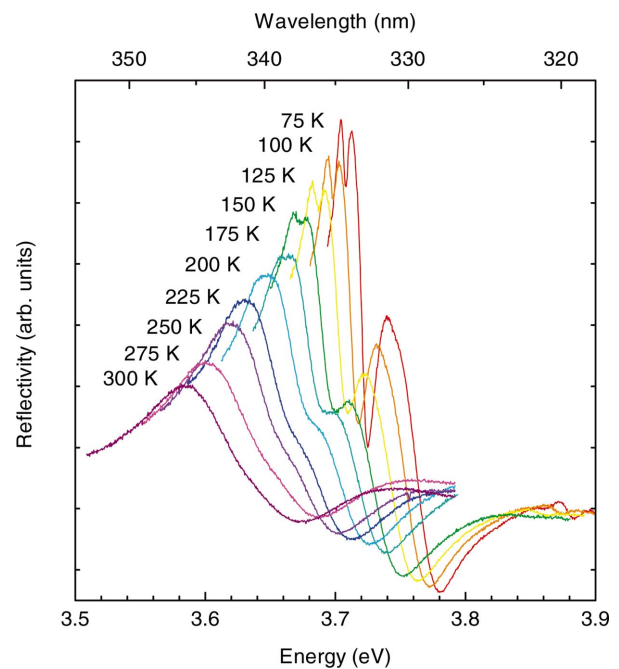


FIG. 4. (Color) Temperature evolution of the unpolarized reflectivity. A freestanding 3D sample with thickness  $\approx 10 \mu\text{m}$  shows strong  $E_{\parallel c}$  resonances superimposed on those from Fig. 3(a).

tion is even larger than Fig. 3, and only a rising edge of the A peak can be observed, even for the etched samples. Reflectivity shows that all four peaks from Fig. 3(b) are replicated in  $E_{\parallel c}$  at a few tens of meV higher energy, and with larger oscillator strength. This is seen in the temperature-dependent unpolarized reflectivity (Fig. 4). At 75 K, the  $E_{\parallel a}$  A and B reflectivity is still evident at 3.71 and 3.75 eV, but the spectrum is dominated by the  $E_{\parallel c}$  dispersive features at 3.73 and 3.76 eV. As the temperature is raised to 300 K, the reflectivity broadens and redshifts until only the  $E_{\parallel c}$  A and B features are discernible at 3.61 and 3.65 eV.

At UV and visible energies lower than 3.7 eV, the low-temperature material is transparent. The multiple reflection interference peaks were measured out to the visible region, where the interference order number<sup>13,14</sup> was identified by measuring Brewster's angle at two wavelengths. The refractive index for  $E_{\parallel c}$  and  $E_{\parallel a}$  was then identified at the series of transmission maxima in Fig. 5. The result shows an optically dense and birefringent media, consistent with the strong band-edge absorption.

In the 1D platelets, where ZnTe has been networked into linear chains, a strong absorption edge was also seen, as shown in Fig. 3(b), but with a significant 0.6 eV additional blueshift in the transition energy. From the low energy tail, the absorption edge was estimated to be 4.4 eV at low temperature and 4.1 eV at room temperature. The dichroism and birefringence, in directions parallel and orthogonal to the linear chains, were also comparable to that of the 3D sample.

#### IV. DISCUSSION

This optical anisotropy, as well as the discrete features in the electronic density of states that are now observable are

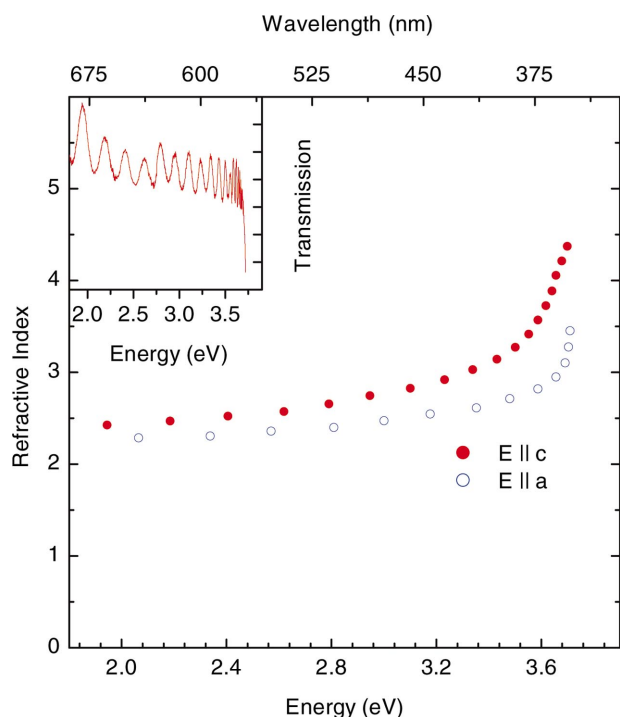


FIG. 5. (Color) Refractive index data in the below-gap region of the 3D freestanding sample. Solid and open points are  $E_{\parallel c}$  and  $E_{\parallel a}$  at 1.6 K. Broadband transmission spectrum for  $E_{\parallel c}$  is shown in the inset.

due to the high quality of the present crystals. Previous measurements on similar materials were limited to diffuse reflectance, or transmission of liquid suspensions of randomly oriented nanocrystals.<sup>6,9,11,15</sup> Those results established the approximate energetic position of the absorption edge, but the features were typically broad, and no symmetry information was possible. In interpreting the new data, care must be taken in describing the properties of hybrid semiconductors in terms of confinement-modified bulk properties. A semiconductor monolayer or chain, bounded by high potential barriers, will not be amenable to effective-mass approximations. The situation may be further complicated by different semiconductor crystal phases, or even stoichiometry that changes because of the layer terminations, as in bulk  $\text{PbI}_2$  which becomes hybrid  $\text{PbI}_4$ .<sup>4</sup> Hypothetically, the “monolayer multiple quantum well” could instead be treated as a completely new, homogeneous, organometallic compound. However, the observations made in the present study argue for the contrary. Ethylenediamine has been extensively studied in hybrids, with no strong optical resonances in the region of interest. The structural measurements<sup>5</sup> depicted in Fig. 1 show that en is incorporated as an intact chain, bonded not to other en molecules, but only to Zn ions along the stacking direction, resulting in a some distortion of the monolayer compared to an ideal (110) “slice” of bulk ZnTe. The stoichiometry of the ZnTe is unchanged.

By considering the confinement of this monolayer and its reduced symmetry relative to bulk ZnTe, the measured excitonic peaks at A and B, plus the two additional features at C and D can be interpreted. Reduction to quasi-two dimensions will remove the degeneracy of the zincblende  $\Gamma_8$  valence

band, splitting the exciton into A and B excitons, as seen in Fig. 3. This is analogous to the crystal field splitting in wurtzite GaN, or to the valence band splitting in GaAs quantum wells. Because our monolayer is in the (110) plane, in contrast to the above examples, it need not show a two-dimensional isotropy of absorption and refraction, despite being sectioned from a cubic crystal. Thus the observed optical anisotropy is consistent with the  $D_{2h}$  point group of the hybrid structure.<sup>5</sup>

The weak reflectivity features C and D are assigned to the absorption edge of the quasi-2D continuum for each valence band, combined with their unresolved 2s and higher exciton states. The  $\Gamma$ -point spin-orbit energy is discounted since in bulk ZnTe it is 0.9 eV,<sup>16</sup> much larger than the energy range studied here. While continuum absorption edges are not often seen in reflectivity, they have been observed in the perovskite hybrids.<sup>17</sup> There, the absorption edge signature was found to be more pronounced because of a very strong oscillator strength, similar to that observed in our present structures.

This very strong optical absorption and the massive blueshift of the band edge are the most striking properties of  $\beta\text{-ZnTe(en)}_{1/2}$ , and they both result from the confined environment of the ZnTe monolayer. When the ZnTe slice is removed from the infinite bulk and placed between two insulating layers, its electronic properties are altered to an extent that is unprecedented with conventional quantum wells. The very large absorption is especially noteworthy if one considers the low stacking density of monolayers in the  $b$  direction of Fig. 1(a). It may be understood by considering the combined effects of dielectric confinement<sup>4,18</sup> and quantum (electronic) confinement. When the dielectric constant of the barrier material is lower than that of the well, screening of the Coulomb attraction is reduced, resulting in a much stronger binding energy, smaller Bohr radius, and stronger oscillator strength inside the well. To obtain well and barrier materials with very different dielectric constants would be difficult using deposition techniques, but it occurs readily in this hybrid system. The binding energies,  $E_b$ , in Fig. 3(a) are 0.12 and 0.13 eV for the A and B excitons,  $\sim 10$  times larger than their bulk value of 13 meV<sup>19</sup> and comparable to what has been seen in hybrid  $\text{PbI}_4$ .<sup>4</sup> A large  $E_b$  is also evidenced by Fig. 4 which shows strong excitonic features up to 300 K.

Similarly, the large refractive index enhancement measured near the A exciton is a result of two factors: the large oscillator strength, and its 4 meV linewidth which is sharper than that observed in any previously studied material of this type. The birefringence  $n_c - n_a$  is  $\sim 0.25$  in the visible, or 10% of the average index, making it similar to commercially important materials like calcite and YVO. Such large birefringent optical materials have recently been used in the implementation of high-performance multilayer coatings.<sup>20</sup> The present measurements are not sensitive to the index orthogonal to the planes, however it is very likely different also, as the crystal is expected to be biaxial from its symmetry.

The massive blueshift of the absorption edges exhibited by our two hybrid samples is due to electronic confinement of the ZnTe. Although a monolayer or chain cannot be treated with an effective mass or a dielectric constant, it is

known that the concept of electronic quantum confinement, applied on an atomic scale, can indeed result in very large blue shifts on the order of 1 eV.<sup>5,9,11</sup> The *A* exciton in Fig. 3(a) is 1.34 eV above the low-temperature bulk ZnTe exciton energy of 2.38 eV (Ref. 21), and in the higher-confinement 1D sample, this blueshift is  $\sim 2.0$  eV, yielding a remarkably large range of band-gap tunability for a *single* inorganic material system. In diffuse reflectance measurements of the absorption edge,<sup>6</sup> we have consistently observed these large blueshifts in over 30 such compounds that encompass 1D, 2D, and 3D structures of both wires and planes in different II–VI inorganics. This would not be practical in a deposition-grown monolayer superlattice such as GaAs/AlAs due to layer-width fluctuations<sup>22</sup> and coupling through the much smaller potential barriers. In quantum dot research, these constraints have long been avoided by use of chemical synthesis techniques that yield an inorganic semiconductor particle embedded in an organic capping layer<sup>23</sup> that passivates the surface and prevents aggregation. Thus our hybrid materials might be regarded as an extension of the capping technique. However, the diamine spacers in the present material play a much more important role. They form a host network for an extended periodic array of inorganic semiconductor

segments, resulting in a material that has no inherent structural size limitation, e.g., a hybrid structure can easily be tens of microns thick. The success of this scheme is seen in the coexistence of very sharp linewidths and a giant blueshift, which would be unattainable with any kind of layer width fluctuation. By contrast, the hybrid semiconductor has its layer width built into the lattice periodicity. These unique features, combined with their simplicity of manufacture and wide range of possible components, dimensions and bonding schemes, including fully covalent layering, make  $\beta$ -ZnTe(en)<sub>1/2</sub> and its analogs appear remarkably versatile for optoelectronic applications.

#### ACKNOWLEDGMENTS

The work was supported by the U.S. Department of Energy, Office of Sciences, Basic Energy Sciences and the Fundamental and Exploratory Research Program of the NCPV under Contract No. DEAC36-99GO10337. X.Y.H. and J.L. would like to acknowledge the National Science Foundation for its partial support (DMR-0094872) to this work.

\*Electronic mail: brian\_fluegel@nrel.gov

<sup>1</sup>V. M. Agranovich, D. M. Basko, G. C. La Rocca, and F. Bassani, *J. Phys.: Condens. Matter* **10**, 9369 (1998).

<sup>2</sup>T. Goto, N. Ohshima, T. A. Mousdis, and G. C. Papavassiliou, *Solid State Commun.* **117**, 13 (2001).

<sup>3</sup>D. B. Mitzi, C. D. Dimitrakopoulos, and L. L. Kosbar, *Chem. Mater.* **13**, 3728 (2001).

<sup>4</sup>X. Hong, T. Ishihara, and A. V. Nurmikko, *Phys. Rev. B* **45**, 6961 (1992).

<sup>5</sup>X. Huang, J. Li, and H. Fu, *J. Am. Chem. Soc.* **122**, 8789 (2000).

<sup>6</sup>X. Huang, J. Li, Y. Zhang, and A. Mascarenhas, *J. Am. Chem. Soc.* **125**, 7049 (2003).

<sup>7</sup>X.-Y. Huang, H. R. Heulings IV, V. Le, and J. Li, *Chem. Mater.* **13**, 3754 (2001).

<sup>8</sup>H. R. Heulings IV, X.-Y. Huang, J. Li, T. Yuen, and C. L. Lin, *Nano Lett.* **1**, 521 (2001).

<sup>9</sup>S.-H. Yu, J. Yang, Y.-T. Qian, and M. Yoshimura, *Chem. Phys. Lett.* **361**, 362 (2002).

<sup>10</sup>X. Chen, H. Xu, N. Xu, F. Zhao, W. Lin, G. Lin, Y. Fu, Z. Huang, H. Wang, and M. Wu, *Inorg. Chem.* **42**, 3100 (2003).

<sup>11</sup>Z.-X. Deng, L. Li, and Y. Li, *Inorg. Chem.* **42**, 2331 (2003).

<sup>12</sup>R. LeToullec, N. Piccioli, and J. C. Chervin, *Phys. Rev. B* **22**, 6162 (1980).

<sup>13</sup>A. A. Sirenko, P. Etchegoin, A. Fainstein, K. Eberl, and M. Cardona, *Phys. Status Solidi B* **215**, 241 (1999).

<sup>14</sup>Y. Zhang, B. Fluegel, J. F. Geisz, J. M. Olson, F. Alsina, and A. Duda, *Solid State Commun.* **104**, 577 (1997).

<sup>15</sup>Y. Dong, Q. Peng, R. Wang, and Y. Li, *Inorg. Chem.* **42**, 1794 (2003).

<sup>16</sup>J. P. Walter, M. L. Cohen, Y. Petroff, and M. Balkanski, *Phys. Rev. B* **1**, 2661 (1970).

<sup>17</sup>T. Ishihara, J. Takahashi, and T. Goto, *Phys. Rev. B* **42**, 11099 (1990).

<sup>18</sup>L. V. Keldysh, *JETP Lett.* **29**, 658 (1979).

<sup>19</sup>G. N. Aliev, O. S. Koshchug, and R. P. Seisyan, *Phys. Solid State* **36**, 203 (1994).

<sup>20</sup>M. J. Weber, C. A. Stover, L. R. Gilbert, T. J. Nevitt, and A. J. Ouder Kirk, *Science* **287**, 2451 (2000).

<sup>21</sup>H. Leiderer, A. Supritz, M. Silberbauer, M. Lindner, W. Kuhn, H. P. Wagner, and W. Gebhardt, *Semicond. Sci. Technol.* **6**, A101 (1991).

<sup>22</sup>J. H. Li, S. C. Moss, Y. Zhang, A. Mascarenhas, L. N. Pfeiffer, K. W. West, W. K. Ge, and J. Bai, *Phys. Rev. Lett.* **91**, 106103 (2003).

<sup>23</sup>X. Peng, L. Manna, W. Yang, J. Wickham, E. Scher, A. Kadavanch, and A. P. Alivisatos, *Nature (London)* **404**, 59 (2000).